

# The Impact of the Asian Summer Monsoon Circulation on the Tropopause

YUTIAN WU

*Department of Earth, Atmospheric, and Planetary Sciences, Purdue University, West Lafayette, Indiana*

TIFFANY A. SHAW

*Department of the Geophysical Sciences, University of Chicago, Chicago, Illinois*

(Manuscript received 7 March 2016, in final form 21 August 2016)

## ABSTRACT

Previous studies have identified two important features of summertime thermodynamics: 1) a significant correlation between the low-level distribution of equivalent potential temperature  $\theta_e$  and the potential temperature  $\theta$  of the extratropical tropopause and 2) a northwestward shift of the maximum tropopause  $\theta$  relative to the maximum low-level  $\theta_e$ . Here, the authors hypothesize these two features occur because of the Asian monsoon circulation. The hypothesis is examined using a set of idealized prescribed sea surface temperature (SST) aquaplanet simulations. Simulations with a zonally symmetric background climate exhibit a weak moisture–tropopause correlation. A significant correlation and northwestward shift occurs when a zonal wave-1 SST perturbation is introduced in the Northern Hemisphere subtropics. The equivalent zonal-mean subtropical warming does not produce a significant correlation.

A mechanism is proposed to explain the moisture–tropopause connection that involves the circulation response to zonally asymmetric surface heating and its impact on the tropopause defined by the 2-potential-vorticity-unit (PVU;  $1 \text{ PVU} = 10^{-6} \text{ K kg}^{-1} \text{ m}^2 \text{ s}^{-1}$ ) surface. While the circulation response to diabatic heating is well known, here the focus is on the implications for the tropopause. Consistent with previous research, surface heating increases the low-level  $\theta_e$  and produces low-level convergence and a cyclonic circulation. The low-level convergence is coupled with upper-level divergence via convection and produces an upper-level anticyclonic circulation consistent with Sverdrup balance. The anticyclonic vorticity lowers the PV northwest of the surface heating via Rossby wave dynamics. The decreased PV leads to a northwestward shift of the 2-PVU surface on fixed pressure levels. The  $\theta$  value to the northwest of the surface heating is higher, and consequently the maximum tropopause  $\theta$  increases.

## 1. Introduction

The tropopause is a transition layer that separates the turbulently mixed troposphere and stably stratified stratosphere. This transition in static stability is also associated with a sharp gradient of potential vorticity and chemical constituents such as water vapor and ozone (e.g., Holton et al. 1995; Kunz et al. 2011). The processes that determine the global tropopause, the extratropical tropopause in particular, are not fully understood. Previous studies have suggested that the extratropical tropopause is related to moist processes in the troposphere (e.g., Jukes 2000; Frierson et al. 2006; Frierson 2008;

Korty and Schneider 2007; Schneider and O’Gorman 2008; Frierson and Davis 2011; Czaja and Blunt 2011) and large-scale stratospheric dynamics (e.g., Birner 2010). More specifically the thermal stratification of the extratropical atmosphere, or the vertical gradient of equivalent potential temperature  $\theta_e$ , has been related to low-level  $\theta_e$  variability, which can be further related to the meridional gradient of  $\theta_e$  near the surface consistent with baroclinic instability (e.g., Jukes 2000; Frierson et al. 2006; Frierson 2008; Schneider and O’Gorman 2008; Frierson and Davis 2011).

The role of the moist dynamics can also be interpreted as follows: low-level air parcels move upward and poleward along moist isentropes to the tropopause level, and moist isentropes converge to dry isentropes in the upper troposphere. Thus, some connection is expected between the low-level  $\theta_e$  and tropopause  $\theta$ . A recent study by Wu and Pauluis (2014) related the potential

---

*Corresponding author address:* Yutian Wu, Department of Earth, Atmospheric, and Planetary Sciences, Purdue University, 550 Stadium Mall Drive, West Lafayette, IN 47907.  
E-mail: wu640@purdue.edu

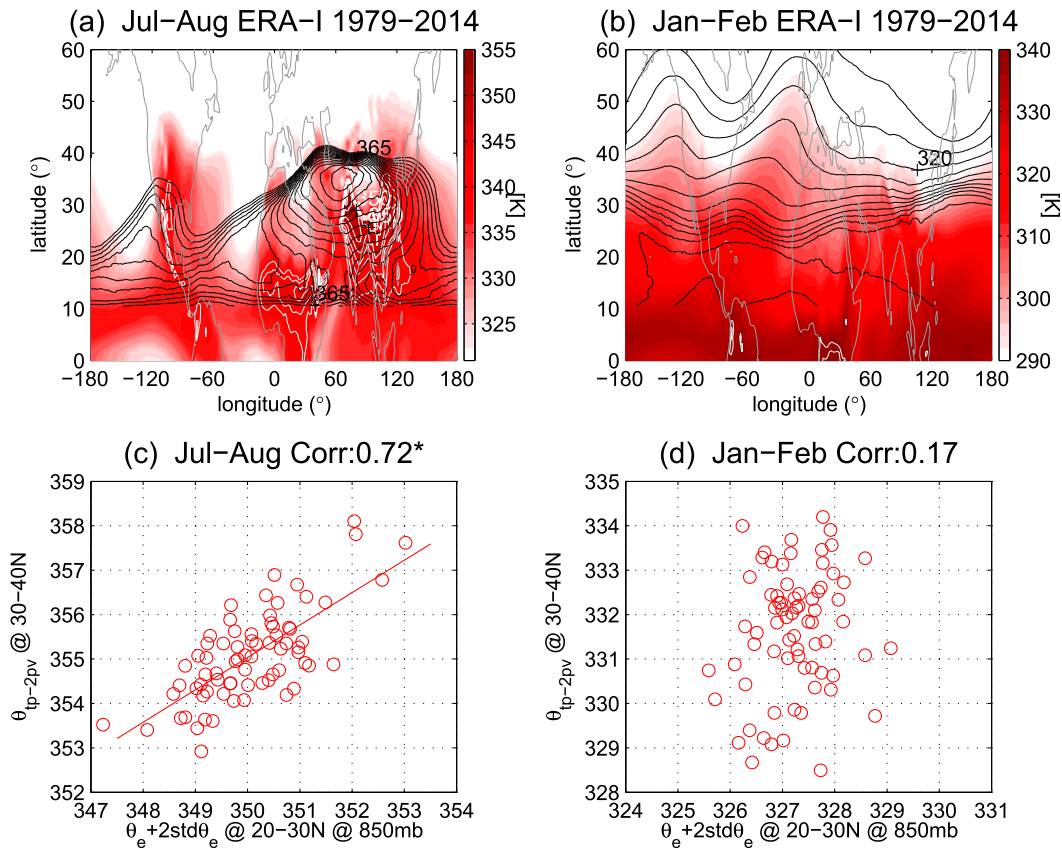


FIG. 1. The potential temperature on the 2-PVU tropopause  $\theta_{tp-2pv}$  (black contours) and 850-mb  $\theta_e$  (color shadings) during (a) July and August and (b) January and February in ERA-Interim. Note the different color scales in (a),(b). The white contours highlight the 850-mb  $\theta_e$  values greater than 340 K with contour interval (CI) = 2 K in (a),(b). The black contours in (a) highlight the  $\theta_{tp-2pv}$  values greater than 355 K, with CI = 1 K. The black contours in (b) plot the  $\theta_{tp-2pv}$  values greater than 310 K, with CI = 5 K. The  $\theta_{tp-2pv}$  is plotted poleward of about 10° N. Scatterplot of 850-mb zonal-mean  $\theta_e + 2\sqrt{\theta_e'^2}$ , averaged over 20°–30° N, vs zonal-mean  $\theta_{tp-2pv}$ , averaged over 30°–40° N, during months of (c) July and August and (d) January and February of 1979–2014. The \* indicates that the correlation is statistically significant at the 95% level. A linear regression curve is plotted on (c).

temperature  $\theta$  of the extratropical tropopause to the daily distribution of low-level  $\theta_e$ . Specifically, in the zonal mean, the tropopause  $\theta_{tp}$  was related to the mean plus two standard deviations of the low-level  $\theta_e$ :

$$\overline{\theta_{tp}} = \overline{\theta_{e,srf}} + 2\sqrt{\overline{\theta_{e,srf}'^2}}, \quad (1)$$

where the overbar denotes time and zonal average and prime denotes deviation from time and zonal average (see Wu and Pauluis 2014 for derivations). Here we use  $\hat{\theta}_e$  to denote  $\overline{\theta_{e,srf}} + 2\sqrt{\overline{\theta_{e,srf}'^2}}$ . The term  $\hat{\theta}_e$  includes both the mean and eddy component of low-level  $\theta_e$ , and the eddy component consists of both stationary and transient eddies and highlights the spatial and temporal variance of low-level  $\theta_e$  in determining the tropopause  $\theta$ . The moisture–tropopause relationship, as in Eq. (1), suggests that the potential temperature of the tropopause

is determined by low-level  $\hat{\theta}_e$ . This is also consistent with the conclusion of Pauluis et al. (2011), who argued that the thermal stratification of the atmosphere is related to the eddy-induced fluctuations of equivalent potential temperature. Wu and Pauluis (2014, 2015) found that this moisture–tropopause relationship works well to explain the annual cycle of the extratropical tropopause across all the seasons in both reanalysis datasets and phase 5 of the Coupled Model Intercomparison Project (CMIP5) multimodel mean. However, the relationship is only significant interannually (i.e., for year-to-year variability) during Northern Hemisphere (NH) summer in reanalysis datasets (Wu and Pauluis 2014).

The seasonal moisture–tropopause relationships during NH summer and NH winter are shown in Fig. 1. Here we define summer as July and August and winter as January and February. We simply refer to 850-hPa  $\theta_e$  as the low-level  $\theta_e$ , and it is maximized over South Asia

during NH summer (shown in Fig. 1a). In addition, the potential temperature of the tropopause, defined as the 2-potential-vorticity-unit (PVU;  $1 \text{ PVU} = 10^{-6} \text{ K kg}^{-1} \text{ m}^2 \text{ s}^{-1}$ ) surface, maximizes over the Tibetan Plateau and is located to the northwest of the low-level  $\theta_e$  maximum. A similar feature exists over the North American monsoon region but it has a smaller magnitude. Figure 1c shows a scatterplot of the monthly (July and August) zonal-mean tropopause potential temperature  $\overline{\theta_{\text{tp}}}$ , averaged over  $30^\circ$ – $40^\circ$  N where  $\theta_{\text{tp}}$  is maximized, and zonal-mean low-level  $\hat{\theta}_e$ , averaged over  $20^\circ$ – $30^\circ$  N where  $\theta_e$  is maximized. It can be seen that the variability of the tropopause  $\theta$  is correlated with the low-level  $\hat{\theta}_e$  during NH summer (e.g., years with large low-level  $\hat{\theta}_e$  tend to have large tropopause  $\theta$ ). On the contrary, the tropopause  $\theta$  is more zonally symmetric in NH winter, and there is no statistically significant correlation in the year-to-year variability between the tropopause  $\theta$  and low-level  $\hat{\theta}_e$ , as shown in Figs. 1b,d. The same conclusion holds at other latitudes in the NH subtropics (not shown). A weak correlation is found in the Southern Hemisphere (SH) (see Figs. 5 and 6 of Wu and Pauluis 2014).

Since the correlation between low-level  $\theta_e$  and tropopause  $\theta$  only exists during NH summer, we hypothesize that the Asian summer monsoon plays a critical role in determining the mean pattern and variability of the tropopause. Previous studies have shown that low-level equivalent potential temperature is coupled to precipitation and upper-tropospheric temperature via upright convection (Nie et al. 2010) and that diabatic heating due to convection drives a Rossby wave response involving a low-level cyclone and upper-level anticyclone (Gill 1980; Rodwell and Hoskins 1996; Wang and Ting 1999; Rodwell and Hoskins 2001) around South Asia. In the upper troposphere the Rossby wave response leads to interhemispheric coupling (Schneider and Watterson 1984; Shaw 2014). Previous studies have also shown the influence of the Asian summer monsoon circulation on the tropopause and on the troposphere–stratosphere exchange (e.g., Dethof et al. 1999; Gettelman et al. 2004; Dessler and Sherwood 2004; Randel and Park 2006; Randel et al. 2010; Son et al. 2011; Randel et al. 2015). In particular, Son et al. (2011) examined the global tropopause using the global positioning system radio occultation measurements from the Constellation Observing System for Meteorology, Ionosphere and Climate (COSMIC) Formosa Satellite Mission 3 (FORMOSAT-3) and found significant intraseasonal variability of the tropopause over the Tibetan Plateau during NH summer.

In this study, we hypothesize that the monsoon and its zonally asymmetric surface heating are important for the moisture–tropopause relationship, and we test this

hypothesis using a set of idealized prescribed sea surface temperature (SST) aquaplanet model experiments following Shaw (2014). In particular, we address the following questions: Why is there a strong moisture–tropopause correlation during NH summer? Does the moisture–tropopause correlation depend on the presence of zonal asymmetries associated with the monsoon? How does the low-level cyclonic circulation and upper-level anticyclonic circulation affect the tropopause?

This paper is organized as follows. In section 2 we describe the reanalysis dataset and idealized model experiments used in this study. In section 3 we quantify the moisture–tropopause correlation in reanalysis data and in idealized aquaplanet simulations. We also propose a mechanism to explain the link between low-level moisture and the tropopause. Section 4 concludes the paper.

## 2. Reanalysis and idealized model experiments

We use ERA-Interim (Dee et al. 2011) from 1979 to 2014 to quantify the moisture–tropopause relationship. As in Fig. 1, we focus on the relationship during NH summer (July and August) and NH winter (January and February).<sup>1</sup> The results are robust among most reanalysis datasets (Wu and Pauluis 2014).

To assess the impact of the monsoon on the tropopause, we make use of a set of idealized aquaplanet model experiments using the NCAR Community Atmospheric Model version 5 (CAM5) (Neale et al. 2012) from Shaw (2014). The control (CTRL) experiment prescribes a zonally symmetric SST with maximum SST shifted to  $10^\circ\text{N}$  [see Qobs SST distribution as in Eq. (1) of Neale and Hoskins (2000) with a modification that shifts maximum SST to  $10^\circ\text{N}$ ]. To test our hypothesis about the importance of the monsoon, we add a subtropical wave-1 SST perturbation (WAVE1) that mimics the NH subtropical land–ocean heating contrast. The wave-1 SST perturbation is centered at  $30^\circ\text{N}$  and has a maximum of 7.5 K [see Eq. (6) of Neale and Hoskins (2000) with a modification that shifts maximum SST anomaly to  $30^\circ\text{N}$ ]. Shaw (2014) showed that a subtropical zonally asymmetric warming in an aquaplanet simulation produces a monsoon-like circulation. Figure 2a shows the SST pattern for the CTRL experiment, and the SST pattern for the WAVE1 experiment is the sum of Figs. 2a and 2b. Both CTRL and WAVE1 simulations are run for 10 years, and the analysis is based

<sup>1</sup> We use both July and August, instead of the mean of July and August, in order to increase the sample size. But the conclusions remain similar with the average of July and August. Similarly, we use both January and February for winter.

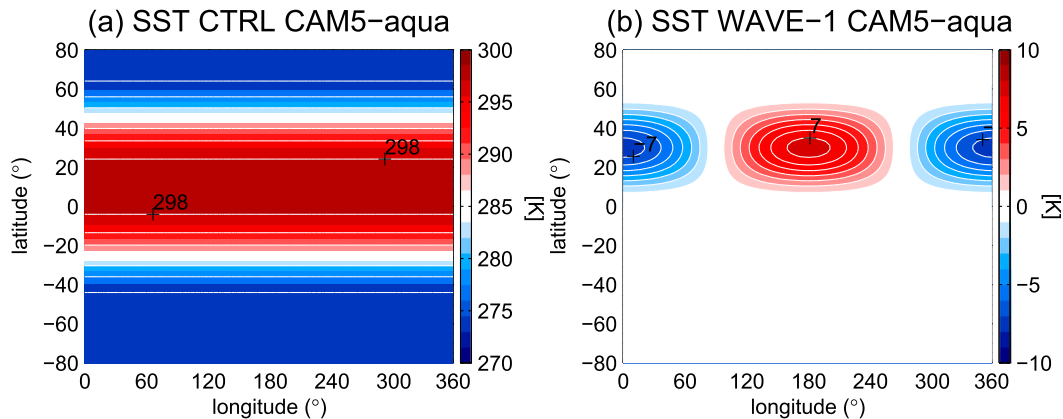


FIG. 2. CAM5 aquaplanet model configuration with (a) zonally symmetric Qobs SST distribution with maximum SST located at 10° N and (b) wave-1 SST perturbation located at 30° N. The CI is 4 K in (a) and 1 K in (b).

on the last 8 years. Since the aquaplanet model experiments are integrated with perpetual equinox insolation, the variation from one month to another is considered as the interannual variability.

The main goal of this paper is to examine the moisture–tropopause relationship [Eq. (1)] and its underlying dynamical mechanism in idealized aquaplanet model experiments. We estimate the left-hand side of Eq. (1), or the extratropical tropopause potential temperature, as the  $\theta$  value at the 2-PVU surface following Holton et al. (1995) and Wu and Pauluis (2014, 2015). The potential vorticity is calculated as  $PV = -g(f + \zeta)(\partial\theta/\partial p)$ , where  $f$  is the Coriolis parameter and  $\zeta$  is the relative vorticity. We estimate the right-hand side of Eq. (1), or the zonal-mean low-level  $\hat{\theta}_e$ , by using daily temperature and specific humidity at 850 mb and  $\theta_e$  formula in Eq. (4.5.11) of Emanuel (1994). Similar results are found using other levels near the surface (not shown). The significance of the correlation coefficient between low-level moisture and tropopause  $\theta$  is quantified using a bootstrap method. The bootstrap method independently resamples the results with replacement and each time calculates a new correlation coefficient using the new samples, and we repeat the process 1000 times. A confidence interval is calculated using 2.5th and 97.5th percentiles of the resampled correlation coefficients, and the correlation coefficient is considered statistically significant at the 95% level if the confidence interval does not include zero.

### 3. Results

#### a. Idealized model experiments

We begin by assessing the moisture–tropopause correlation in the idealized aquaplanet model experiments following Eq. (1). In the CTRL experiment, there is no

statistically significant correlation between the low-level  $\hat{\theta}_e$  and tropopause  $\theta$  (Fig. 3a). This is reminiscent of the ERA-Interim results for NH winter (shown in Fig. 1d). A significant moisture–tropopause correlation occurs in the WAVE1 experiment (Fig. 3b; the correlation coefficient is 0.73 and is statistically significant at the 95% level using the bootstrap method) and is reminiscent of the ERA-Interim results for NH summer (Fig. 1c). To quantify the importance of zonally localized warming, we performed an additional perturbation experiment involving a 2.5-K subtropical zonal-mean warming perturbation, which is equivalent to a localized zonal mean over the 7.5-K wave-1 warming region (90°–270°E in Fig. 2b). The zonal-mean warming perturbation did not produce a significant moisture–tropopause correlation (not shown).

The values of low-level  $\hat{\theta}_e$  and tropopause  $\theta$  increase dramatically in the WAVE1 experiment. For example, the range of low-level  $\hat{\theta}_e$  is 10 K in the WAVE1 experiment, while it is only about 3 K in CTRL. Similar changes are seen for the tropopause potential temperature. The range of low-level  $\hat{\theta}_e$  in the WAVE1 experiment is 342–352 K, which is in reasonable agreement with the reanalysis data during summertime (shown in Fig. 1c). Recall that the low-level  $\hat{\theta}_e$  includes both the mean and eddy components (two standard deviations) of  $\theta_e$ . Figures 3c–f separate the contribution into the mean and eddy components. In CTRL, neither the mean nor the eddy components of  $\theta_e$  are statistically significantly correlated with the tropopause  $\theta$  (Figs. 3c,e). However, the strong moisture–tropopause correlation in the WAVE1 experiment is due to both the mean and eddy components of low-level  $\theta_e$  (Figs. 3d,f). In addition, this moisture–tropopause correlation in the WAVE1 experiment occurs in a broad range of NH subtropics, while nearly no correlation is found in this region in CTRL (Figs. 4a,b).

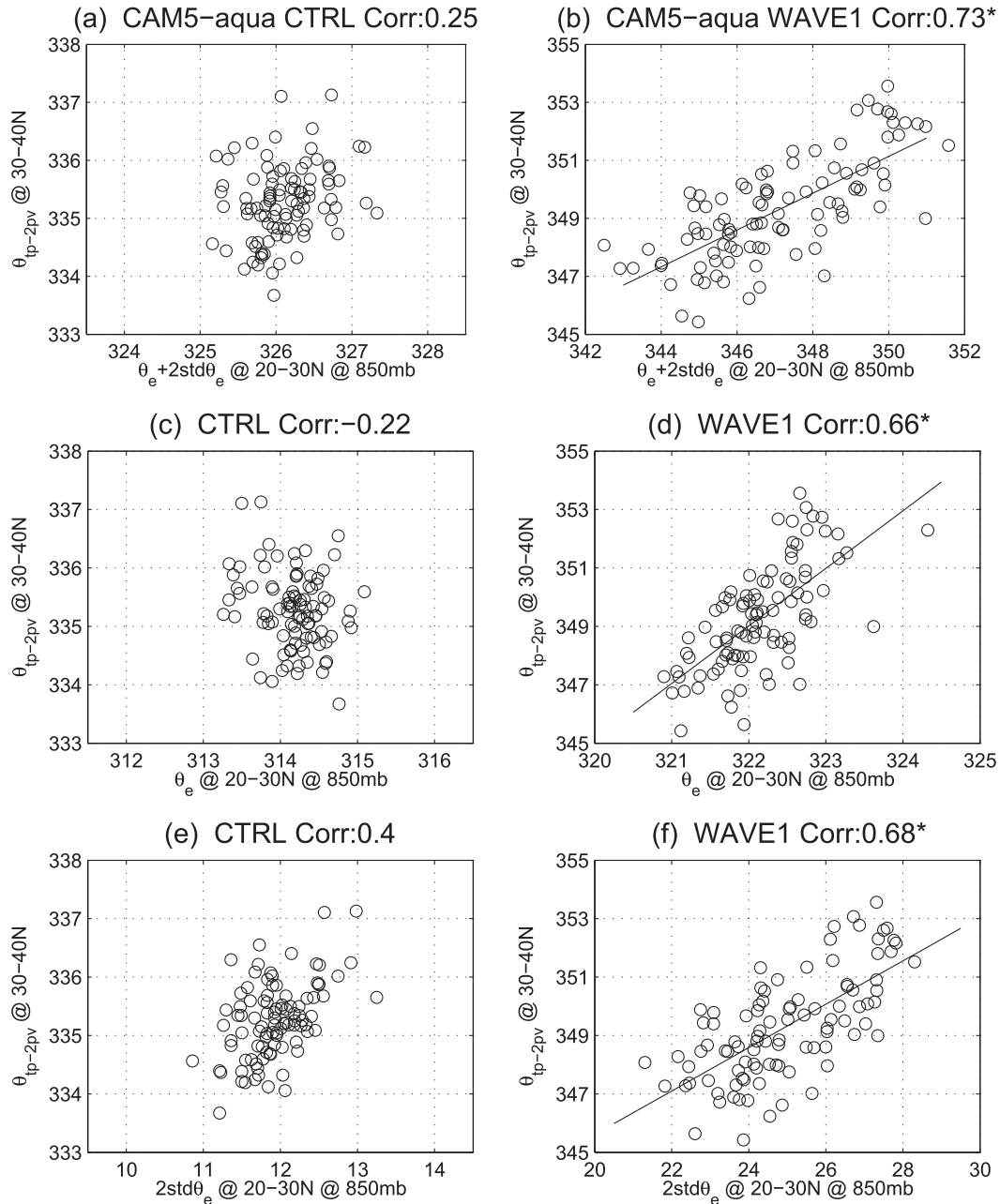


FIG. 3. Scatterplot of 850-mb zonal-mean  $\theta_e + 2\sqrt{\theta_e^2}$ , averaged over  $20^\circ\text{--}30^\circ\text{N}$ , vs zonal-mean  $\theta_{\text{tp-2pv}}$ , averaged over  $30^\circ\text{--}40^\circ\text{N}$ , in CAM5 aquaplanet (a) CTRL and (b) WAVE1 perturbation experiments. The \* indicates the correlation is statistically significant at the 95% level. (c)–(f) As in (a),(b), but separating the mean (c),(d)  $\theta_e$  and (e),(f)  $2\sqrt{\theta_e^2}$  components for the CTRL and WAVE1 experiments. A linear regression curve is plotted in cases with statistically significant correlation.

In addition to the correlation between low-level moisture and tropopause  $\theta$ , we also find that the thermal stratification of the northern subtropics is connected to the eddy variation of equivalent potential temperature in the WAVE1 experiment. The difference of the mean tropopause  $\theta$  and mean low-level  $\theta_e$ , which can be considered as the thermal stratification of the

atmosphere or the moist static stability, is significantly correlated with the low-level eddy  $\theta_e$  in the WAVE1 experiment (Fig. 5a). The eddy  $\theta_e$  is dominated by the planetary-scale wave-1 contribution (Fig. 5c), consistent with the zonal wave-1 SST forcing. The observed thermal stratification in the NH summer subtropics is also correlated with the low-level eddy  $\theta_e$ , primarily wave-1

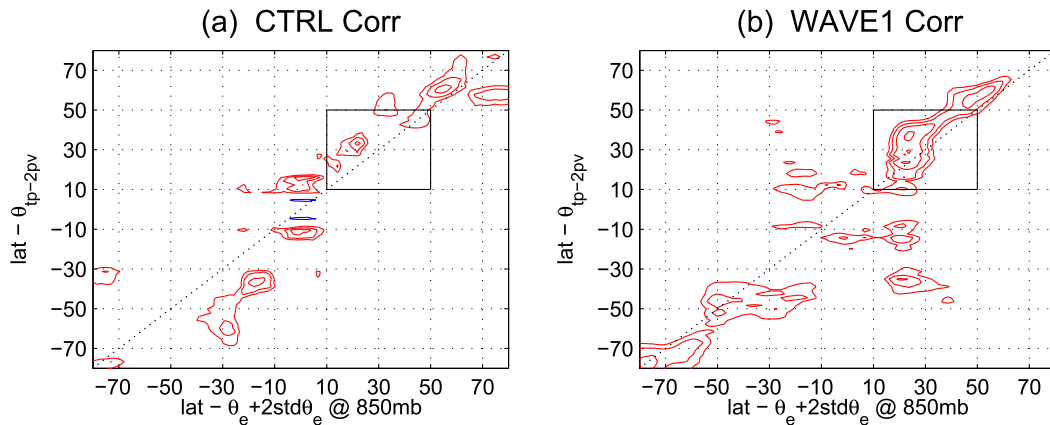


FIG. 4. The moisture-tropopause correlation across various latitudes in (a) CTRL and (b) WAVE1 experiments and with contours above 0.4 and CI = 0.1. The main region of interest, 10°–50° N, is highlighted by a black box.

and wave-2 components in ERA-Interim (Figs. 5b,d), consistent with the results from idealized experiments. This confirms that planetary-scale eddies play an important role in determining the thermal stratification of

the atmosphere during NH summer. The dominance of wave 1 and wave 2 in the real atmosphere is in agreement with the results of Shaw and Pauluis (2012), who emphasized the importance of latent heat transport by

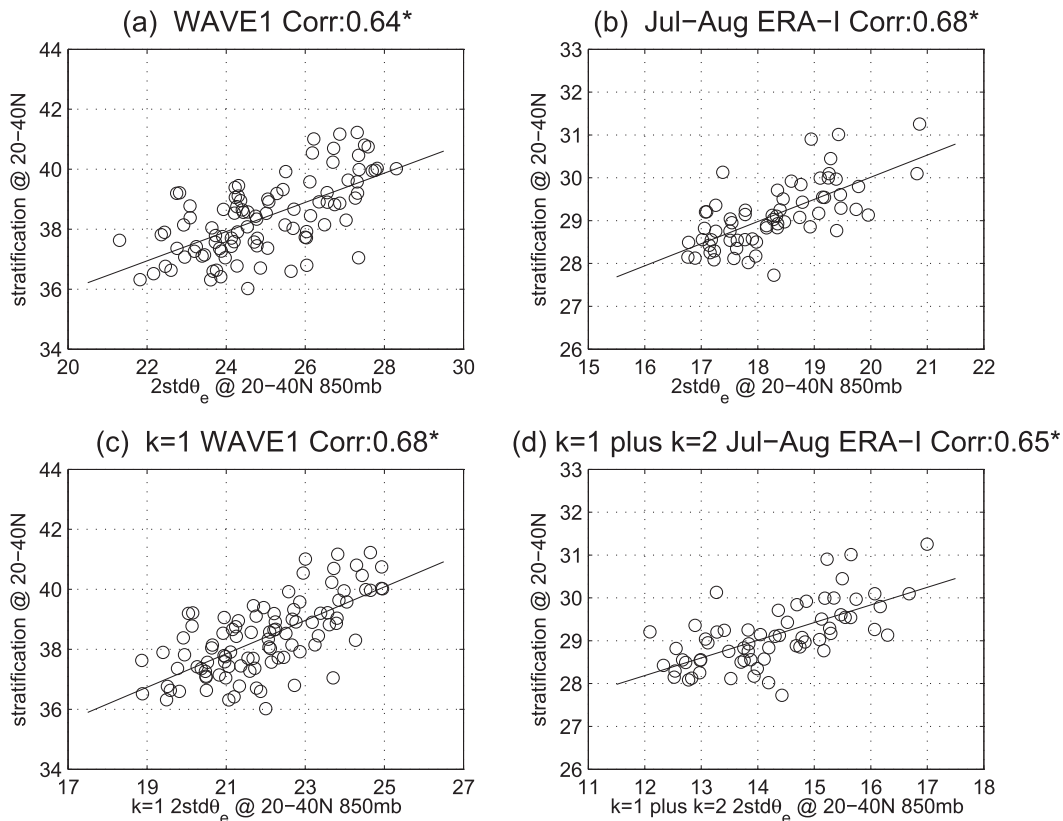


FIG. 5. Scatterplot of vertical stratification (the same for all four subplots) vs (a) 850-mb  $2\sqrt{\theta_e^2}$  and (c) wave-1 component of  $2\sqrt{\theta_e^2}$  averaged over 20°–40° N in CAM5 aquaplanet WAVE1 experiment. The vertical stratification is calculated as the difference between  $\theta_{tp-2pv}$  and 850-mb  $\theta_e$ . (b),(d) As in (a),(c), but (b) during July and August in ERA-Interim and (d) the sum of wave-1 and wave-2 contributions. A linear regression curve is plotted in cases with statistically significant correlation.

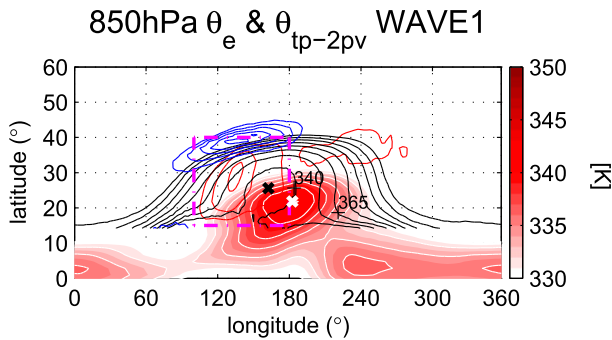


FIG. 6. In CAM5 aquaplanet WAVE1 experiment, 850-hPa  $\theta_e$  (color shadings and white contours; CI = 2 K), its month-to-month standard deviation (red contours) and tropopause  $\theta_{tp-2pv}$  (black contours; CI = 2 K), and its month-to-month standard deviation (blue contours). The white and black crosses highlight the maximum of 850-hPa  $\theta_e$  and  $\theta_{tp-2pv}$ , respectively. The pink dashed-dotted box highlights the region with large variability of low-level  $\theta_e$ .

planetary-scale eddies during NH summer associated with the Asian and North American monsoons.

Previous studies have connected the vertical stratification of the extratropical atmosphere to the meridional gradient of  $\theta_e$  (e.g., Jukes 2000; Frierson et al. 2006; Frierson 2008; Schneider and O’Gorman 2008; Frierson and Davis 2011). For example, Frierson and Davis (2011) (hereinafter referred to as FD11) showed that the vertical stratification and meridional gradient of  $\theta_e$  in the extratropics are correlated in the NASA MERRA dataset. However, the meridional gradient of  $\theta_e$  does not fully explain the thermal stratification of the atmosphere during NH summer, as shown in Fig. 3 of FD11. FD11 argued different mechanisms at play between the largely ocean-covered SH and land-covered NH. Here we suggest that planetary-scale eddies associated with the monsoon during NH summer are critical and need to be taken into consideration in understanding the stratification of the atmosphere.

In addition to the moisture–tropopause correlation, the WAVE1 experiment also captures the northwestward shift of maximum tropopause potential temperature relative to maximum low-level  $\theta_e$ . Figure 6 shows the mean pattern and variability of the low-level (850 hPa) mean  $\theta_e$  and tropopause  $\theta$  in the WAVE1 experiment. The maximum mean  $\theta_e$  near the surface (shown in color shadings and white contours in Fig. 6) is located above the warm SST perturbation. The mean tropopause  $\theta$  (shown in black contours in Fig. 6) is not collocated with but is shifted to the northwest of the mean low-level  $\theta_e$  by about 20° longitude and 4° latitude. This is consistent with the reanalysis results shown in Fig. 1a. In addition, the variability of low-level  $\theta_e$  (shown in red contours in Fig. 6) is found mostly to the northwest

of the mean  $\theta_e$  and, to a lesser extent, to the northeast side. Furthermore, the variability of tropopause  $\theta$  (shown in blue contours in Fig. 6) is also maximized to the northwest of the low-level  $\theta_e$  variability. This northwestward shift of maximum  $\theta$  on the 2-PVU tropopause also occurs for  $\theta$  on the thermal tropopause, which is identified as the lowest level where the temperature lapse rate drops below  $2 \text{ K km}^{-1}$  (WMO 1957) in both idealized experiments and ERA-Interim (not shown).

### b. Mechanism

The results of the previous section demonstrate that a moisture–tropopause relationship, similar to that observed during NH summer, is present in an aquaplanet simulation with a subtropical zonally asymmetric surface heating. In addition, the tropopause potential temperature is located to the northwest of the low-level equivalent potential temperature, consistent with the feature in reanalysis during NH summer.

We hypothesize that the moisture–tropopause relationship, including the northwestward shift of maximum  $\theta$  on the 2-PVU tropopause, is a consequence of the Rossby wave response to surface heating. Rodwell and Hoskins (1996, 2001) proposed the monsoon–desert mechanism that links the Mediterranean and east Sahara Deserts to the Asian monsoon via a Rossby wave response to diabatic heating. South Asian diabatic heating drives ascent, low-level convergence, and low-level cyclonic circulation. Divergence in the upper troposphere drives an anticyclonic circulation via Sverdrup balance, consistent with Gill (1980). Descent occurs to the west (over the Mediterranean and eastern Sahara) as a result of Rossby wave dynamics and is balanced adiabatically via temperature advection. While the circulation response to diabatic heating is well known, here we focus on the implications for the tropopause and show that the circulation response to surface heating can explain the increase of tropopause potential temperature and its westward shift relative to surface heating in the WAVE1 experiment.

We begin by establishing the monsoon–desert relationship in the WAVE1 experiment. A low-level cyclonic circulation (shown in Fig. 7a; southward of about 35°N and within 120°–240° longitude) and an ascent (shown in Fig. 7b) occur slightly to the west of the surface heating (SST warming). An anticyclonic circulation exists above the low-level cyclone and is located to the northwest relative to the low-level cyclone (shown in Fig. 7c). Ascent occurs over the warm SST perturbation and large low-level  $\theta_e$ , whereas descent occurs to the northwest consistent with the Rossby wave response. The vertical and horizontal flow are coupled via Sverdrup balance; that is,  $\beta v \approx f(\partial\omega/\partial p)$ , where  $f$  is the

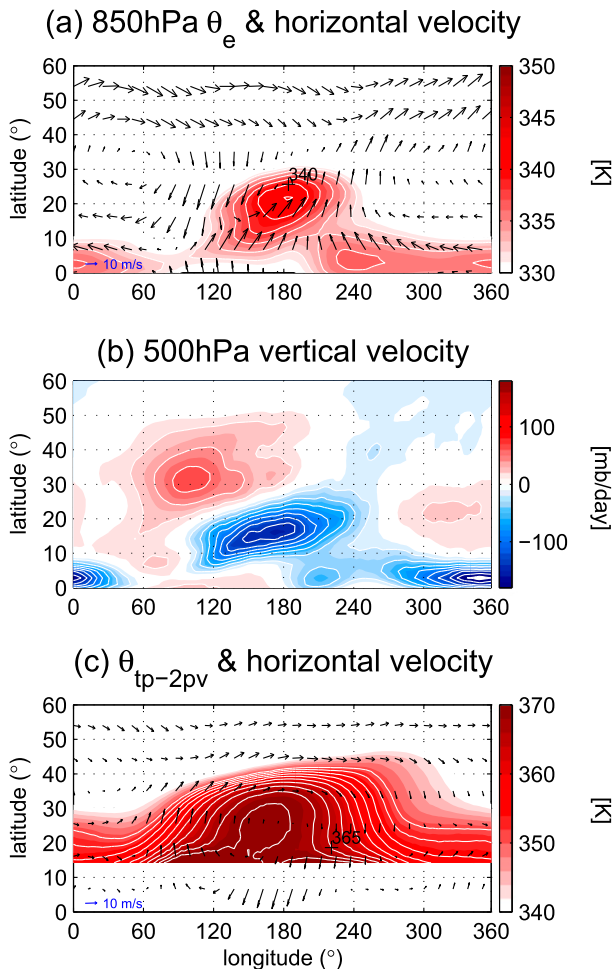


FIG. 7. In CAM5 aquaplanet WAVE1 experiment, (a) 850-hPa  $\theta_e$  (color shadings in unit of K; CI = 2 K) and 850-hPa horizontal velocity vectors, (b) 500-hPa vertical velocity  $\omega$  (color shadings in unit of  $\text{mb day}^{-1}$ ; CI =  $20 \text{ mb day}^{-1}$ ), and (c) tropopause  $\theta_{\text{tp-2pv}}$  (color shadings in unit of K; CI = 2 K) and 150-hPa horizontal velocity vectors.

Coriolis parameter,  $\beta$  is its meridional gradient,  $v$  is meridional velocity, and  $\omega$  is vertical velocity (this coupling is not shown).

The monsoon–desert mechanism can affect the 2-PVU tropopause in different ways. For example, surface warming affects stratification via convection, and the Rossby wave response produces upper-level anticyclonic relative vorticity  $\zeta$ , which modifies PV. To determine the factors that dominate the change of  $\theta$  on the 2-PVU tropopause between the CTRL and WAVE1 experiments, we separately assess the role of  $\theta$  versus PV changes as follows. If we evaluate the CTRL  $\theta$  on the 2-PVU surface from WAVE1 and thus isolate the change of tropopause  $\theta$  due to the change of PV surface (shown in Fig. 8b), there is a clear northwestward shift of the maximum  $\theta$ . If we evaluate the WAVE1  $\theta$  on the

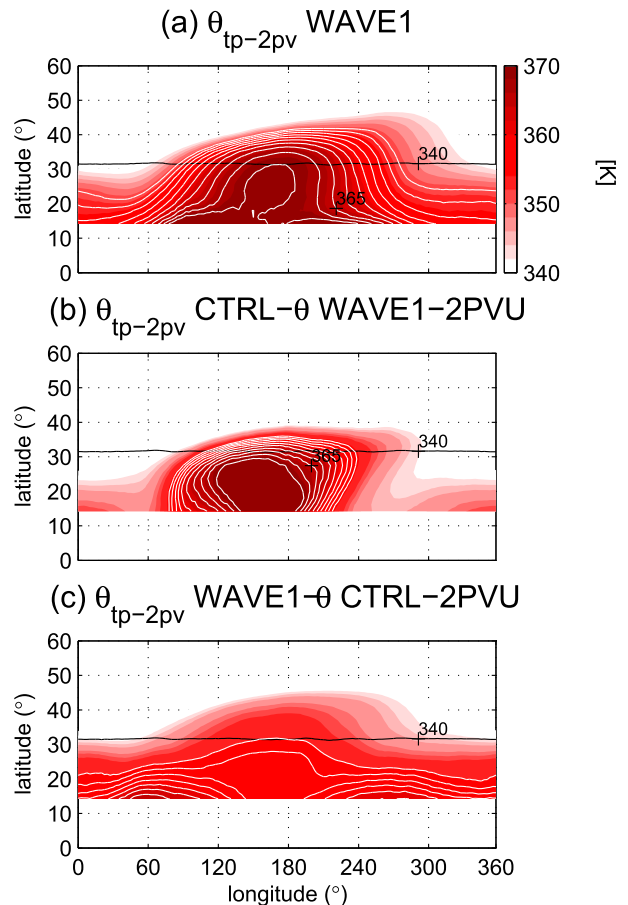


FIG. 8. (a) The potential temperature on the 2-PVU surface in the WAVE1 experiment, (b) calculated using CTRL  $\theta$  and WAVE1 2 PVU, and (c) calculated using WAVE1  $\theta$  and CTRL 2 PVU in color shadings and white contours with CI = 2 K for (a)–(c). The black contour highlights the 340-K isentrope in CTRL.

2 PVU from CTRL (shown in Fig. 8c), the results do not involve a significant change in the tropopause  $\theta$  near the region of surface heating. This suggests that the increase and northwestward shift of maximum tropopause potential temperature in the WAVE1 experiment is largely a consequence of the northwestward shift of the 2-PVU surface in response to surface warming. Recall that in NH climatology, PV increases monotonically with  $\theta$  at each latitude (see Fig. 3a of Hoskins 1991). As the 2-PVU surface moves to the northwest, the potential temperature increases and leads to a northwestward shift of maximum tropopause potential temperature relative to the low-level heating.

Next we examine the processes contributing to the change of PV between the CTRL and WAVE1 experiment on pressure surfaces. Hoskins (1991) argued that PV values decrease above the heating maximum and conservation of mass-weighted PV requires an increase of mass, leading to divergence and anticyclonic

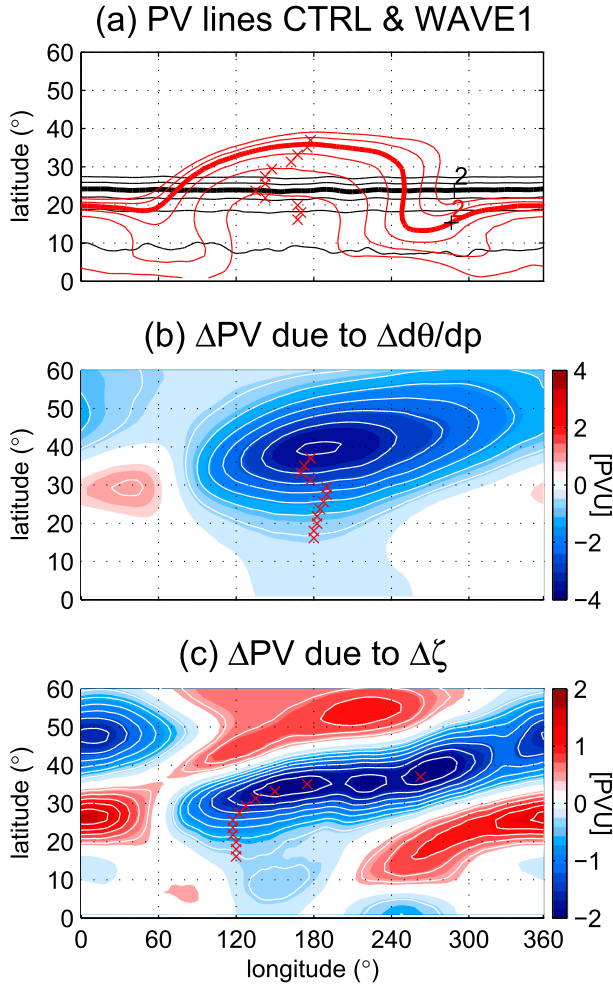


FIG. 9. (a) PV at 150 hPa in the CTRL (black contours) and WAVE1 (red contours) experiments with CI = 0.5 PVU. Thick contours highlight the 2-PVU surface. The decomposition of the change of PV (WAVE1 minus CTRL) (b) due to the change of stratification [i.e.,  $-g(f + \zeta_c)\delta(\partial\theta/\partial p)$ ] and (c) due to the change of relative vorticity [i.e.,  $-g(f + \delta\zeta)(\partial\theta/\partial p)$ ]. The red crosses highlight the minimum at each latitude of 15°–40° N in (a) WAVE1 PV, (b)  $-g(f + \zeta_c)\delta(\partial\theta/\partial p) + PV_c$ , and (c)  $-g(f + \delta\zeta)(\partial\theta/\partial p) + PV_c$ . The CI is 0.5 PVU for (b) and 0.25 PVU for (c).

circulation in the upper troposphere (see Fig. 2 of Hoskins 1991). In our WAVE1 experiment, we also see a decrease of PV in response to surface heating in the upper troposphere leading to a northern shift of the 2-PVU surface between 120° and 240°E relative to its zonally symmetric position in CTRL (Fig. 9a). In addition to the northern shift, the PV surfaces in the WAVE1 experiment also shift westward (see red crosses in Fig. 9a). To understand the cause of the northwestward shift of the PV surfaces, we decompose the change of PV into contributions due to the change of relative vorticity and due to the change of stratification. The decomposition is written as follows:

$$\delta PV \approx -g(f + \zeta_c)\delta\left(\frac{\partial\theta}{\partial p}\right) - g(f + \delta\zeta)\left(\frac{\partial\theta}{\partial p}\right)_c, \quad (2)$$

where  $\delta$  indicates the difference between the CTRL and WAVE1 and subscript  $c$  denotes the CTRL experiment. Figure 9b shows the PV change due to the stratification change, and Fig. 9c shows the PV change due to the vorticity change. The sum of the two changes is in reasonable agreement with the total PV change (i.e., difference between red and black contours in Fig. 9a). The PV change due to the stratification change is symmetric with respect to 180°E and provides a large part of the northward shift of the PV (Fig. 9b), whereas the decrease of PV due to the upper-level anticyclone contributes to the westward shift (Fig. 9c).

As in Hoskins (1991), the diabatic heating decreases the PV values in the upper troposphere. In addition to that, the upper-level anticyclone, which is located to the northwest of the surface heating due to Rossby wave dynamics, also modifies the relative vorticity and PV and shifts the decrease of PV to the west. Since PV increases with latitude and with  $\theta$  in the NH, the potential temperature evaluated at the northwestward-shifted 2-PVU surface increases. Thus, the aquaplanet model results suggest the northwestward shift of maximum  $\theta$  on the 2-PVU tropopause in the WAVE1 experiment is largely determined by the northwestward shift of constant PV surfaces due to the anticyclonic vorticity generated via the Rossby wave response (Fig. 9a).

The Rossby wave mechanism also explains the variability of the tropopause potential temperature. The variability of low-level  $\theta_e$  (pink box in Fig. 6) is located to the northwest of the low-level mean  $\theta_e$ . In addition, the variability of tropopause  $\theta$  is located to the northwest of the low-level  $\theta_e$  variability. Figure 10 shows the regression of low-level circulation and  $\theta_e$ , 500-hPa vertical velocity, upper-level circulation, and tropopause  $\theta$  on the low-level  $\theta_e$  averaged over the pink box. A regression of the circulation onto the low-level  $\theta_e$  variability reveals a low-level cyclone and an upper-level anticyclone (shown in Figs. 10a,c). The ascent is associated with low-level northward flow and descent occurs to the northwest (shown in Figs. 10a–c). Thus, the monsoon–desert relationship affects both the mean and variability of the tropopause primarily through the upper-level anticyclonic circulation response to diabatic heating. The anticyclonic circulation is northwestward of the surface heating because of the Rossby wave dynamics.

Finally we demonstrate the causality of the moisture–tropopause correlation. The low-level  $\theta_e$  (averaged over 100°–260° longitude) is found to lead the tropopause  $\theta$  by

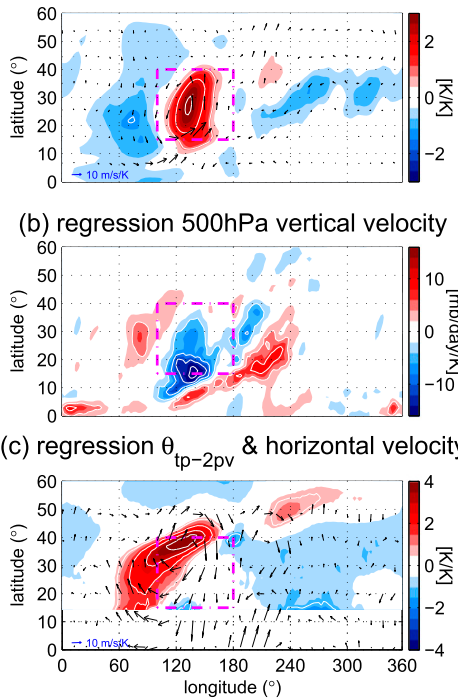
(a) regression 850hPa  $\theta_e$  & horizontal velocity WAVE1

FIG. 10. Similar to Fig. 7, but regression of (a) 850-hPa  $\theta_e$  and 850-hPa horizontal velocity, (b) 500-hPa vertical velocity  $\omega$ , and (c) tropopause  $\theta_{tp-2pv}$  and 150-hPa horizontal velocity on 850-hPa  $\theta_e$ , averaged over the pink dashed-dotted box. The pink dashed-dotted box is the same as one in Fig. 6 and highlights the region with large low-level  $\theta_e$  variability. The CI is 1 for (a),  $4 \text{ mb day}^{-1} \text{ K}^{-1}$  for (b), and 1 for (c).

about 5 days (Fig. 11), and this causality is consistent with the mechanism outlined above.

#### 4. Conclusions and discussion

A statistically significant correlation exists between the distribution of low-level  $\theta_e$  and  $\theta$  on the 2-PVU tropopause during NH summer. This describes the dynamical process that warm and moist air parcels at the lower levels move along moist isentropes to the tropopause level and modulate the tropopause potential temperature. In addition, the maximum tropopause  $\theta$  is located northwest of the maximum low-level  $\theta_e$ . Here we used a set of idealized, prescribed SST, aquaplanet simulations to test the hypothesis that the moisture–tropopause correlation and the westward shift of maximum tropopause  $\theta$  relative to maximum low-level  $\theta_e$  arise as a result of the monsoon circulation driven by zonally asymmetric subtropical surface heating. Here we conclude by addressing the questions we raised in the introduction:

- Why is there a strong moisture–tropopause correlation during NH summer? Does the moisture–tropopause

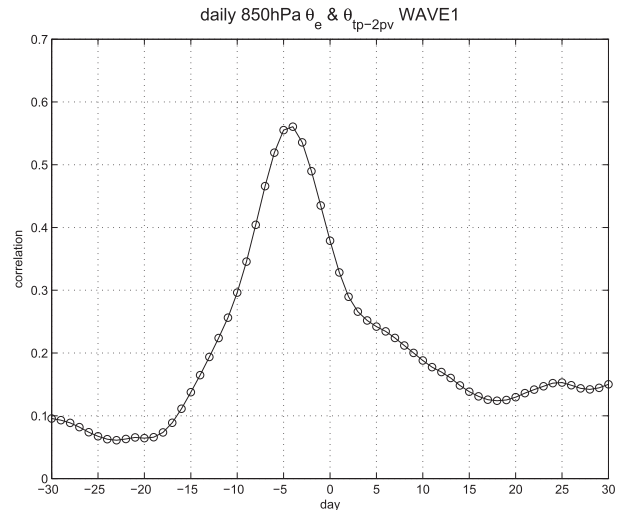


FIG. 11. The cross correlation of daily anomalies from mean 850-mb  $\theta_e$  averaged from  $100^\circ$  to  $260^\circ$  E and  $20^\circ$  to  $30^\circ$  N and tropopause  $\theta_{tp-2pv}$  averaged from  $100^\circ$  to  $260^\circ$  E and  $30^\circ$  to  $40^\circ$  N in the WAVE1 experiment.

correlation depend on the presence of zonal asymmetries associated with the monsoon? The strong moisture–tropopause correlation during NH summer is due to the zonally asymmetric surface heating associated with the summer monsoon. This was demonstrated using the aquaplanet model experiments. A significant correlation occurs in prescribed SST aquaplanet simulations when a subtropical wave-1 surface warming is added to the SST. However, a zonally symmetric aquaplanet simulation with no subtropical warming or zonal-mean perturbation equivalent to the wave-1 warming does not exhibit the moisture–tropopause relationship. We have found that the moisture–tropopause correlation only develops when the warming is of sufficient amplitude in the zonal mean to match the maximum 7.5-K wave-1 forcing (not shown). The results from the idealized aquaplanet simulations confirm the role of the Asian summer monsoon heating in determining the observed moisture–tropopause correlation. In addition, planetary-scale eddies associated with the monsoon play a fundamental role in determining the thermal stratification of the atmosphere.

- How does the low-level cyclonic circulation and upper-level anticyclonic circulation affect the tropopause? The low-level equivalent potential temperature is fundamentally connected to the tropopause via the coupling of low-level heating, cyclonic circulation, upright convection, and upper-level anticyclonic circulation (Rodwell and Hoskins 1996, 2001). Figure 12 summarizes the mechanism in a schematic and shows the monsoon–desert mechanism involving the Rossby

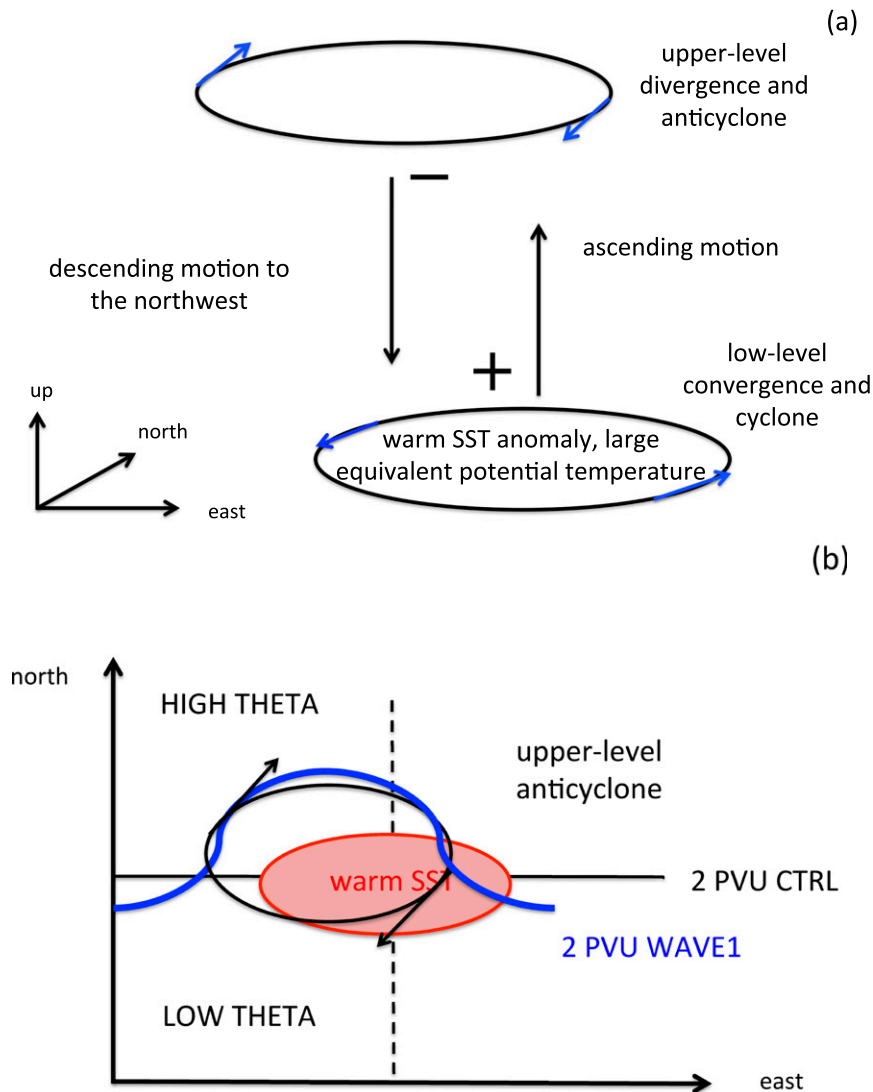


FIG. 12. Schematic of moisture–tropopause connection associated with monsoon circulation. Monsoon–desert response to surface heating involving low-level cyclone and upper-level anticyclone indicated by black ellipses. The  $\pm$  signs indicate changes in PV due to diabatic heating following Hoskins (1991). Black vertical arrows indicate vertical motion. This follows Rodwell and Hoskins (1996, 2001); see text for explanation. (b) Cross section of PV changes due to surface warming. Anticyclonic circulation (black ellipse) shifts 2-PVU surface (blue line) to the northwest where  $\theta$  is larger.

wave response to diabatic heating (Gill 1980; Highwood and Hoskins 1998; Rodwell and Hoskins 1996, 2001). The imposed warm SST perturbation induces large  $\theta_e$  near the surface and a thermally direct circulation with ascent above the warm SST (Fig. 12a). The low-level convergence drives a cyclonic circulation. Divergence occurs in the upper troposphere, which drives an upper-level anticyclone via Sverdrup balance. Descent occurs to the west because of westward propagation of the Rossby wave and is balanced adiabatically via temperature advection. Our results,

which connect the monsoon–desert mechanism to the tropopause, are summarized in Fig. 12b. The dominant impact of the monsoon–desert relationship on the tropopause occurs via anticyclonic vorticity, which lowers the PV to the northwest of the low-level heating. Because  $\theta$  increases as you move north on the 2-PVU tropopause, as the 2-PVU surface moves northwestward, the potential temperature at the perturbed 2-PVU surface increases, causing an increase and northwestward shift of the maximum tropopause potential temperature relative to the low-level heating.

Our results are in agreement with previous observational studies that highlighted the importance of the Asian monsoon circulation on the tropopause and troposphere–stratosphere transport (e.g., Dethof et al. 1999; Gettelman et al. 2004; Dessler and Sherwood 2004; Randel and Park 2006; Randel et al. 2010; Son et al. 2011; Randel et al. 2015). For example, Randel et al. (2015) analyzed subseasonal variability of the stratospheric water vapor in the summer monsoon regions using the *Aura* Microwave Limb Sounder satellite observations. They found that stronger convection in the monsoon regions leads to colder tropopause temperature in the subtropical lower stratosphere, enhanced dehydration within the anticyclonic circulation, and a relatively dry stratosphere. The correlation involving large low-level  $\theta_e$  and large tropopause  $\theta$  examined here (Fig. 1c) supports the result of stronger convection and less stratospheric water vapor, as found in Randel et al. (2015). The fact we have identified a larger tropopause  $\theta$  as compared to the control is primarily due to a rise of the tropopause height despite a decrease of the temperature (not shown). The decrease of tropopause pressure largely contributes to the northwest shift of maximum tropopause  $\theta$ , which is consistent with the role of the circulation. In addition, Randel et al. (2015) showed enhanced convection tends to precede the stratospheric dry anomalies by about 0–10 days. This time scale is consistent with the aquaplanet experiments (Fig. 11).

Our results on the northwestward shift of the maximum tropopause potential temperature are not contradictory with the theory of convective quasi equilibrium. The theory of convective quasi equilibrium suggests subcloud-layer  $\theta_e$  and saturation  $\theta_e$  in the free troposphere in convecting regions should be collocated (Arakawa and Schubert 1974; Emanuel et al. 1994). Boos and Kuang (2010) and Nie et al. (2010) examined thermodynamics in the monsoon regions and found that the maxima of free-tropospheric temperature and subcloud  $\theta_e$  indeed are closely collocated. Boos and Kuang (2010) considered the vertical average of 175–450 hPa in the free troposphere, whereas our focus is the tropopause located at about 100–200 hPa. In fact, as shown in Fig. 4 of Nie et al. (2010), the maximum of  $\theta_e$  is nearly collocated in the vertical column below 200 hPa but is shifted to the north above 200 hPa, and thus our results do not contradict Nie et al. (2010).

While the aquaplanet model experiments provide significant insights into the mechanisms responsible for the moisture–tropopause relationship, there are a couple of caveats worth mentioning. First, convection in CAM5, or state-of-the-art atmospheric general circulation models (AGCMs) in general, is highly parameterized. Second, we did not include the effect of topography.

Fu et al. (2006) demonstrated that the deep convection occurs frequently over the Tibetan Plateau and could effectively overshoot water vapor and polluted air into the stratosphere. Boos and Kuang (2010) also demonstrated the importance of the Himalayas for monsoon precipitation and circulation. Topography may play a role in the tropopause: as the westerly flow ascends along the topography, an upper-level anticyclonic circulation is expected to be generated owing to conservation of PV. However, Liu et al. (2007) argued that the upper-level anticyclone is predominately forced by diabatic heating and weakly by orographic forcing. Third, we did not explain why the tropopause potential temperature is related to a large fluctuation of  $\theta_e$  near the surface—more specifically, two standard deviations of  $\theta_e$ . Although the moisture–tropopause relationship suggests upward and poleward movement of moist air parcels from the surface to the tropopause level, most deep convective updrafts entrain air with lower  $\theta_e$  during ascent (Folkens and Martin 2005). It is likely that undiluted ascent, and thus conservation of  $\theta_e$ , is only true for a small fraction of the moist air parcels, which may explain why the tropopause is related to two standard deviations of low-level  $\theta_e$ . Future work is needed for a more thorough understanding.

Overall we have demonstrated the Asian summer monsoon circulation plays an important role in determining the mean pattern and variability of the tropopause, and prescribed SST aquaplanet simulations provide a useful framework for studying the underlying mechanisms.

*Acknowledgments.* The authors thank the reviewers for their helpful comments. The authors are thankful to Olivier Pauluis, Tapio Schneider, Bill Randel, Kai Zhang, and Pengfei Zhang for helpful discussion. YW is supported, in part, by the National Science Foundation (NSF). TAS acknowledges support from the David and Lucile Packard Foundation, the Alfred P. Sloan Foundation, and the NSF (AGS-1538944).

## REFERENCES

- Arakawa, A., and W. H. Schubert, 1974: Interaction of a cumulus cloud ensemble with the large-scale environment, part I. *J. Atmos. Sci.*, **31**, 674–701, doi:10.1175/1520-0469(1974)031<0674:IOACCE>2.0.CO;2.
- Birner, T., 2010: Residual circulation and tropopause structure. *J. Atmos. Sci.*, **67**, 2582–2600, doi:10.1175/2010JAS3287.1.
- Boos, W. R., and Z. Kuang, 2010: Dominant control of the South Asian monsoon by orographic insulation versus plateau heating. *Nature*, **463**, 218–222, doi:10.1038/nature08707.
- Czaja, A., and N. Blunt, 2011: A new mechanism for ocean–atmosphere coupling in midlatitudes. *Quart. J. Roy. Meteor. Soc.*, **137**, 1095–1101, doi:10.1002/qj.814.

- Dee, D. P., and Coauthors, 2011: The ERA-Interim reanalysis: Configuration and performance of the data assimilation system. *Quart. J. Roy. Meteor. Soc.*, **137**, 553–597, doi:10.1002/qj.828.
- Dessler, A. E., and S. C. Sherwood, 2004: Effect of convection on the summertime extratropical lower stratosphere. *J. Geophys. Res.*, **109**, D23301, doi:10.1029/2004JD005209.
- Dethof, A., A. O'Neill, J. M. Slingo, and H. G. J. Smit, 1999: A mechanism for moistening the lower stratosphere involving the Asian summer monsoon. *Quart. J. Roy. Meteor. Soc.*, **125**, 1079–1106, doi:10.1002/qj.1999.49712555602.
- Emanuel, K. A., 1994: *Atmospheric Convection*. Oxford University Press, 592 pp.
- , J. D. Neelin, and C. S. Bretherton, 1994: On large-scale circulations in convecting atmospheres. *Quart. J. Roy. Meteor. Soc.*, **120**, 1111–1143, doi:10.1002/qj.49712051902.
- Folkins, I., and R. V. Martin, 2005: The vertical structure of tropical convection and its impact on the budgets of water vapor and ozone. *J. Atmos. Sci.*, **62**, 1560–1573, doi:10.1175/JAS3407.1.
- Frierson, D. M. W., 2008: Midlatitude static stability in simple and comprehensive general circulation models. *J. Atmos. Sci.*, **65**, 1049–1062, doi:10.1175/2007JAS2373.1.
- , and N. A. Davis, 2011: The seasonal cycle of midlatitude static stability over land and ocean in global reanalyses. *Geophys. Res. Lett.*, **38**, L13803, doi:10.1029/2011GL047747.
- , I. M. Held, and P. Zurita-Gotor, 2006: A gray-radiation aquaplanet moist GCM. Part I: Static stability and eddy scale. *J. Atmos. Sci.*, **63**, 2548–2566, doi:10.1175/JAS3753.1.
- Fu, R., and Coauthors, 2006: Short circuit of water vapor and polluted air to the global stratosphere by convective transport over the Tibetan Plateau. *Proc. Natl. Acad. Sci. USA*, **103**, 5664–5669, doi:10.1073/pnas.0601584103.
- Gottelman, A., D. E. Kinnison, T. J. Dunkerton, and G. P. Brasseur, 2004: Impact of monsoon circulations on the upper troposphere and lower stratosphere. *J. Geophys. Res.*, **109**, D22101, doi:10.1029/2004JD004878.
- Gill, A. E., 1980: Some simple solutions for heat-induced tropical circulation. *Quart. J. Roy. Meteor. Soc.*, **106**, 447–462, doi:10.1002/qj.49710644905.
- Highwood, E. J., and B. J. Hoskins, 1998: The tropical tropopause. *Quart. J. Roy. Meteor. Soc.*, **124**, 1579–1604, doi:10.1002/qj.49712454911.
- Holton, J. R., P. H. Haynes, M. E. McIntyre, A. R. Douglass, R. B. Rood, and L. Pfister, 1995: Stratosphere-troposphere exchange. *Rev. Geophys.*, **33**, 403–440, doi:10.1029/95RG02097.
- Hoskins, B. J., 1991: Towards a PV- $\theta$  view of the general circulation. *Tellus*, **43B**, 27–35, doi:10.3402/tellusb.v43i4.15396.
- Juckes, M. N., 2000: The static stability of the midlatitude troposphere: The relevance of moisture. *J. Atmos. Sci.*, **57**, 3050–3057, doi:10.1175/1520-0469(2000)057<3050:TSSOTM>2.0.CO;2.
- Korty, R. L., and T. Schneider, 2007: A climatology of the tropospheric thermal stratification using saturation potential vorticity. *J. Climate*, **20**, 5977–5991, doi:10.1175/2007JCLI1788.1.
- Kunz, A., L. L. Pan, P. Konopka, D. E. Kinnison, and S. Tilmes, 2011: Chemical and dynamical discontinuity at the extratropical tropopause based on START08 and WACCM analyses. *J. Geophys. Res.*, **116**, D24302, doi:10.1029/2011JD016686.
- Liu, Y. M., B. J. Hoskins, and M. Blackburn, 2007: Impact of Tibetan orography and heating on the summer flow over Asia. *J. Meteor. Soc. Japan*, **85B**, 1–19, doi:10.2151/jmsj.85B.1.
- Neale, R. B., and B. J. Hoskins, 2000: A standard test for AGCMs including their physical parametrizations: I: The proposal. *Atmos. Sci. Lett.*, **1**, 101–107, doi:10.1006/asle.2000.0019.
- , and Coauthors, 2012: Description of the NCAR Community Atmosphere Model (CAM 5.0). NCAR Tech. Note NCAR/TN-486+STR, 282 pp. [Available online at [http://www.cesm.ucar.edu/models/cesm1.0/cam/docs/description/cam5\\_desc.pdf](http://www.cesm.ucar.edu/models/cesm1.0/cam/docs/description/cam5_desc.pdf).]
- Nie, J., W. R. Boos, and Z. Kuang, 2010: Observational evaluation of a convective quasi-equilibrium view of monsoons. *J. Climate*, **23**, 4416–4428, doi:10.1175/2010JCLI3505.1.
- Pauluis, O., T. A. Shaw, and F. Laliberte, 2011: A statistical generalization of the transformed Eulerian-mean circulation for an arbitrary vertical coordinate system. *J. Atmos. Sci.*, **68**, 1766–1783, doi:10.1175/2011JAS3711.1.
- Randel, W. J., and M. Park, 2006: Deep convective influence on the Asian summer monsoon anticyclone and associated tracer variability observed with Atmospheric Infrared Sounder (AIRS). *J. Geophys. Res.*, **111**, D12314, doi:10.1029/2005JD006490.
- , —, L. Emmons, D. Kinnison, P. Bernath, K. Walker, C. Boone, and H. Pumphrey, 2010: Asian monsoon transport of pollution to the stratosphere. *Science*, **328**, 611–613, doi:10.1126/science.1182274.
- , K. Zhang, and R. Fu, 2015: What controls stratospheric water vapor in the NH summer monsoon regions? *J. Geophys. Res. Atmos.*, **120**, 7988–8001, doi:10.1002/2015JD023622.
- Rodwell, M. J., and B. J. Hoskins, 1996: Monsoons and the dynamics of deserts. *Quart. J. Roy. Meteor. Soc.*, **122**, 1385–1404, doi:10.1002/qj.49712253408.
- , and —, 2001: Subtropical anticyclones and summer monsoons. *J. Climate*, **14**, 3192–3211, doi:10.1175/1520-0442(2001)014<3192:SAASM>2.0.CO;2.
- Schneider, E. K., and I. G. Watterson, 1984: Stationary Rossby wave propagation through easterly layers. *J. Atmos. Sci.*, **41**, 2069–2083, doi:10.1175/1520-0469(1984)041<2069:SRWPT>2.0.CO;2.
- Schneider, T., and P. A. O’Gorman, 2008: Moist convection and the thermal stratification of the extratropical troposphere. *J. Atmos. Sci.*, **65**, 3571–3583, doi:10.1175/2008JAS2652.1.
- Shaw, T. A., 2014: On the role of planetary-scale waves in the abrupt seasonal transition of the Northern Hemisphere general circulation. *J. Atmos. Sci.*, **71**, 1724–1746, doi:10.1175/JAS-D-13-0137.1.
- , and O. Pauluis, 2012: Tropical and subtropical meridional latent heat transports by disturbances to the zonal mean and their role in the general circulation. *J. Atmos. Sci.*, **69**, 1872–1889, doi:10.1175/JAS-D-11-0236.1.
- Son, S.-W., N. F. Tandon, and L. M. Polvani, 2011: The fine-scale structure of the global tropopause derived from COSMIC GPS radio occultation measurements. *J. Geophys. Res.*, **116**, D20113, doi:10.1029/2011JD016030.
- Wang, H. L., and M. F. Ting, 1999: Seasonal cycle of the climatological stationary waves in the NCEP–NCAR reanalysis. *J. Atmos. Sci.*, **56**, 3892–3919, doi:10.1175/1520-0469(1999)056<3892:SCOTCS>2.0.CO;2.
- WMO, 1957: Meteorology: A three-dimensional science. *WMO Bull.*, **4**, 134–138.
- Wu, Y., and O. Pauluis, 2014: Midlatitude tropopause and low-level moisture. *J. Atmos. Sci.*, **71**, 1187–1200, doi:10.1175/JAS-D-13-0154.1.
- , and —, 2015: What is the representation of the moisture–tropopause relationship in CMIP5 models? *J. Climate*, **28**, 4877–4889, doi:10.1175/JCLI-D-14-00543.1.